

Self-intermediate scattering function of strongly interacting three-dimensional lattice gases: Time- and wave-vector-dependent tracer diffusion coefficient

Loukas Skarpalezos and Panos Argyrakis

Department of Physics, University of Thessaloniki, 54124 Thessaloniki, Greece

Vyacheslav S. Vikhrenko

Belarusian State Technological University, 13a Sverdlova Str., 220006 Minsk, Belarus

(Received 5 March 2014; published 29 May 2014)

We investigate the self-intermediate scattering function (SISF) in a three-dimensional (3D) cubic lattice fluid (interacting lattice gas) with attractive nearest-neighbor interparticle interactions at a temperature slightly above the critical one by means of Monte Carlo simulations. A special representation of SISF as an exponent of the mean tracer diffusion coefficient multiplied by the geometrical factor and time is considered to highlight memory effects that are included in time and wave-vector dependence of the diffusion coefficient. An analytical expression for the diffusion coefficient is suggested to reproduce the simulation data. It is shown that the particles' mean-square displacement is equal to the time integral of the diffusion coefficient. We make a comparison with the previously considered 2D system on a square lattice. The main difference with the two-dimensional case is that the time dependence of particular characteristics of the tracer diffusion coefficient in the 3D case cannot be described by exponentially decreasing functions, but requires using stretched exponentials with rather small values of exponents, of the order of 0.2. The hydrodynamic values of the tracer diffusion coefficient (in the limit of large times and small wave vectors) defined through SISF simulation results agree well with the results of its direct determination by the mean-square displacement of the particles in the entire range of concentrations and temperatures.

DOI: [10.1103/PhysRevE.89.053318](https://doi.org/10.1103/PhysRevE.89.053318)

PACS number(s): 66.30.-h, 68.43.De

I. INTRODUCTION

For several past decades lattice gases have been widely used for understanding transport phenomena in systems with hopping dynamics [1–5], such as submonolayers on solid surfaces [6,7], ionic crystals [8], intercalation compounds [9,10], electrons on traps [11], etc. However, the main effort was spent to investigate diffusion coefficients in the hydrodynamic regime when the frequency and wave-vector dependence of the diffusion coefficients and other transport quantities was not apparent. The space- and time-dependent density-density correlation functions, their spatial Fourier and time Laplace transforms, the intermediate scattering functions, and the dynamical structure factors, have typically been used in order to understand in more detail the time and spatial behavior of different media dynamic characteristics [12–14]. The general expressions for such functions for lattice gases were incidentally previously discussed [3–5,15], and some theoretical considerations were developed [16–19]. However, the drawback in the examined hydrodynamic regime (low-frequency and small wave-vector limits) has been the fact that important memory effects were not considered in detail. At the same time, information about high-frequency and short-wavelength media characteristics became progressively important for such materials as nanodimensional ceramic or polycrystal materials in order to understand and interpret their behavior or experimental measurements, e.g., by impedance spectroscopy [20,21].

Monte Carlo (MC) simulations of the self-intermediate scattering function (SISF) have been performed [22] for a noninteracting 2D lattice gas using square lattices of size up to 600×600 lattice sites for rather short times, of the order of a hundred Monte Carlo simulation time steps (MCS) or

less. Recently [23], SISF of a lattice fluid (interacting lattice gas) on a square lattice was simulated at slightly supercritical temperatures and memory effects were investigated in detail. We showed there that several time scales govern evolution of a one-particle space-time distribution function starting from ten and up to a thousand MCS. Thus long runs up to 2000 MCS are necessary. The current paper considers the MC simulation results for SISF of the lattice fluid on a simple cubic lattice. The solution of the continuum diffusion equation with the time and distance dependent diffusion coefficient is used for constructing the expression for SISF of a lattice fluid.

II. SELF-INTERMEDIATE SCATTERING FUNCTION AND THE TIME- AND WAVE-VECTOR-DEPENDENT TRACER DIFFUSION COEFFICIENT

The one-particle van Hove space- and time-dependent distribution function can be represented by the expression

$$G_s(\mathbf{r}, t) = \frac{1}{n} \left\langle \sum_{i=1}^n \delta[\mathbf{r} + \mathbf{r}_i(0) - \mathbf{r}_i(t)] \right\rangle, \quad (1)$$

where δ is the Dirac δ function, \mathbf{r} is a radius vector, t is time, and angular brackets denote averaging over a canonical ensemble of n particles. The sum runs over positions of all system particles denoted by radius vector \mathbf{r}_i . For lattice fluids, particles can occupy the lattice sites only. Two- and many-particle occupation of a lattice site is forbidden. The self-part of the distribution function contains positions of the same particle at two different times (zero and t).

We refine the derivation [23] of the expression for the SISF of the lattice fluid considering a continuum homogeneous medium where the function $G_s(\mathbf{r}, t)$ obeys the particle number

conservation equation

$$\frac{\partial G_s(\mathbf{r}, t)}{\partial t} = \frac{\partial}{\partial \mathbf{r}} \cdot \mathbf{J}(\mathbf{r}, t), \quad (2)$$

with the diffusion flux accounting for the spatial dispersion [13,14], that means the flux in a given point is determined by the gradients in all the points of the system

$$\mathbf{J}(\mathbf{r}, t) = - \int_V \hat{\mathbf{D}}_s(\mathbf{r} - \mathbf{r}', t) \cdot \frac{\partial G_s(\mathbf{r}', t)}{\partial \mathbf{r}'} d^3 \mathbf{r}', \quad (3)$$

integration is performed over the volume V of the system, the diffusion coefficients tensor $\hat{\mathbf{D}}_s$ depends on the distance and time. These dependences are evident for a lattice fluid because the preferable movement of a particle back to its previous position (the special vacancy [22]) always exists, thus creating the particular spatial distribution of vacant sites that depends on time after the particle started to move.

The Fourier transform of Eqs. (2) and (3) with accounting of the convolution in the latter equation and subsequent integration over time leads to the expression

$$F_s(\mathbf{k}, t) = F_s(\mathbf{k}, 0) \exp[-\mathbf{k} \cdot \mathbf{D}_s(\mathbf{k}, t) \cdot \mathbf{k}t], \quad (4)$$

where the self-intermediate scattering function $F_s(\mathbf{k}, t)$ is the Fourier transform of the self-part of the one-particle van Hove distribution function, \mathbf{k} is a wave vector, and the mean value of the diffusion coefficients tensor

$$\mathbf{D}_s(\mathbf{k}, t) = \frac{1}{t} \int_0^t \hat{\mathbf{D}}_s(\mathbf{k}, t') dt' \quad (5)$$

is introduced.

For a lattice fluid the initial conditions are taken in the form $G_s(0, 0) = 1$ and $G_s(\mathbf{r} \neq 0, 0) = 0$ and thus $F_s(\mathbf{k}, 0) = 1$. For an isotropic medium the diffusion coefficients tensor is a diagonal tensor and can be represented by the scalar self(tracer)-diffusion coefficient. For a lattice fluid of cubic symmetry the same representation can be used and SISF can be written as

$$F_s(\mathbf{k}, t) = \exp[-D_s(\mathbf{k}, t)\eta(\mathbf{k}t)], \quad (6)$$

where the mean tracer diffusion coefficient $D_s(\mathbf{k}, t)$ appears instead of the tracer diffusion coefficient in [23], and

$$\eta(\mathbf{k}) = \sum_{j=1}^z \frac{1 - \cos(\mathbf{k} \cdot \mathbf{r}_j)}{a^2} \quad (7)$$

is the multiplier that takes into account geometric peculiarities of the lattice, a is a lattice parameter, the sum runs over z nearest-neighbor site positions.

In the nonhydrodynamic regime all memory effects are included into the mean tracer diffusion coefficient $D_s(\mathbf{k}, t)$ that becomes dependent on the wave vector and time. As SISF can easily be calculated in the simulation process, the mean tracer diffusion coefficient is calculated from the expression

$$D_s(\mathbf{k}, t) = - \frac{\ln[F_s(\mathbf{k}, t)]}{\eta(\mathbf{k})t}. \quad (8)$$

The simulation results showed that the diffusion coefficient behaves like the two-dimensional case [23] and may lead us to consider the ansatz:

$$D_s(k, t) = D_{s0}(t) \exp[-B^2(k, t)], \quad (9)$$

where $D_{s0}(t)$ is the time-dependent zero wave-vector mean tracer diffusion coefficient, $B(0, t) = 0$, and the first derivative of $B(k, t)$ over the wave vector at the boundary of the first Brillouin zone is equal to zero as well. D_s and B depend on the orientation of vector \mathbf{k} that will be accounted for by the corresponding dependence of the coefficients representing these quantities.

For B we use the expression that slightly differs from the 2D case,

$$B(k, t) = b(\xi)B_m(t), \quad B_m(t) = B(\xi_m, t), \quad (10)$$

$$\xi = h/\kappa(t), \quad \xi_m = h_{\max}/\kappa(t),$$

$$b(\xi) = b_0[\tanh \xi - \xi / \cosh^2 \xi_m], \quad (11)$$

$$b_0 = 1/[\tanh \xi_m - \xi_m / \cosh^2 \xi_m],$$

where ξ is a dimensionless variable, h is considered as an integer varying between zero and h_{\max} and the characteristic distance κ in the reciprocal space is taken in units of $(2\pi/La)$ for \mathbf{k} directed along a simulated box edge (for other \mathbf{k} directions this unit is shorter because the number of points in the reciprocal space is taken equal to h_{\max} for all k directions), La is the MC simulation box size, and $h_{\max} = L/2$. Also $b(k, t) = b(\xi)$ is a function of ξ that depends on time through the parameter κ only, $b(0) = 0$, and $b(\xi_m) = 1$. B_m is B at the boundary of the first Brillouin zone. The difference from the 2D case is in the $b(\xi)$ function, where $\tanh \xi$ is used instead of $[1 - \exp(-\xi)]$ because $\tanh \xi = 1 - \exp(-\xi)/\cosh \xi$ and thus this function reaches faster its saturation value of 1 with increasing ξ , better representing the k dependence of B . The main anisotropy of the problem is exhibited by function $\eta(k)$. The scaling (7) does not influence the anisotropy of the first Brillouin zone if κ does not depend on the wave-vector orientation. Thus additional anisotropy is reflected by the dependence of $B_m(t)$ and $\kappa(t)$ on the \mathbf{k} direction.

III. SIMULATION PROCEDURES

The initial configuration we used for the Monte Carlo simulations was a simple cubic ($L \times L \times L = 50 \times 50 \times 50$) lattice with periodic boundary conditions, randomly occupied by particles with a coverage (concentration) θ . In this case, the wave vector

$$\mathbf{k} = (2\pi/La)(h\mathbf{i} + m\mathbf{j} + l\mathbf{p}), \quad (12)$$

$$h, m, l = 0, 1, 2, \dots, L/2, \quad h + m + l \neq 0$$

is introduced. Here \mathbf{i} , \mathbf{j} , and \mathbf{p} are the unit vectors in the x , y , and z directions, respectively; $h_{\max} = 25$. We then applied attractive nearest-neighbor interactions between the particles using the following algorithm: the probability p of a randomly chosen particle to jump to a nearest-neighbor empty site depends on the number q of particles occupying the nearest-neighbor sites, and on the temperature T of the system by the following expression:

$$p = e^{-qJ/k_B T}, \quad (13)$$

where J is the interaction parameter which is linked to the critical temperature by the relation $J/k_B T_c \cong 1.128$, where k_B is Boltzmann constant. A Monte Carlo step (MCS) is defined

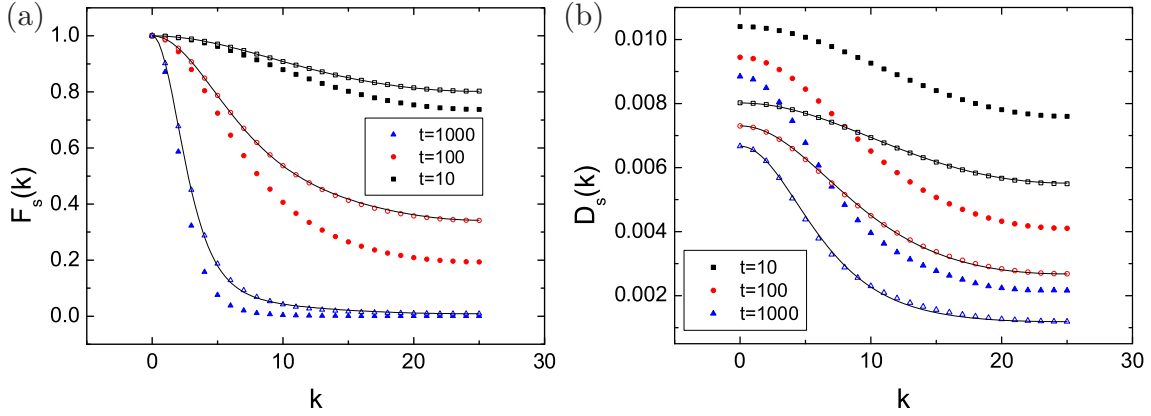


FIG. 1. (Color online) (a) SISF and (b) the mean tracer diffusion coefficient versus the wave vector directed along a cell edge for three different times. $\theta = 0.5$, $T = 1.2T_c$ (full symbols), and $T = 1.05T_c$ (empty symbols). Time t is given in MCS. Solid lines are drawn according to Eqs. (6) and (9) and only for the data of $T = 1.05T_c$ and not for $T = 1.2T_c$ (for clarity in the figures).

by $n = \theta L^3$ trials to move a randomly chosen particle. We let the system evolve until it reaches an equilibrium state (10^4 MCS) before starting to compute at each MCS the value of the self-intermediate scattering function $F_s(\mathbf{k}, t)$ for a time range of 2000 MCS. In fact, we considered the equilibrium state as the initial state for the calculations ($t_0 = 0$). Afterwards, by tracking the position (x_t, y_t, z_t) of every particle at every time step, $F_s(\mathbf{k}, t)$ was readily computed for all the wave vectors $k_x = 2\pi h/La$, $k_y = 2\pi m/La$, and $k_z = 2\pi l/La$:

$$F_s(\mathbf{k}, t) = \frac{1}{n} \sum_i^n \cos\left(\frac{2\pi}{L}[h(x_{i,t} - x_{i,0}) + m(y_{i,t} - y_{i,0}) + l(z_{i,t} - z_{i,0})]\right), \quad (14)$$

where h , m , and l are three integers varying independently from zero to $L/2$ (for symmetry reasons the negative values were not considered) and the particle coordinates are given in units of a . The results obtained are the average of 20 000 independent realizations. Simulations were performed for two temperatures slightly above the critical value ($T = 1.05T_c$ and $T = 1.2T_c$) and for the concentration range θ from 0.3 to 0.8 with a step 0.1. The lattice spacing a was taken equal to 1.

IV. RESULTS AND DISCUSSION

The results for the self-intermediate scattering function are shown in Fig. 1(a), where we plot the SISF vs the wave vector k . The width of the function in k space decreases with time as given by Eqs. (6) and (8), as is always observed in experiments and simulations for liquids and lattice fluids. Initially, the particle is localized in real space that corresponds to complete delocalization in the reciprocal space [$F_s(\mathbf{k}, t = 0) = 1$]. Diffusion leads to delocalization in real space that results in localization in the reciprocal space and the larger the diffusion coefficient the faster localization occurs, and thus at higher temperature the localization in the reciprocal space is faster.

Figure 1(b) demonstrates that the mean tracer diffusion coefficient sharply decreases with k in the region of small k , and then decreases more slowly when k is approaching the boundary of the first Brillouin zone. The tangents are horizontal at $k = 0$ and $k = k_m$, where $k_m = \pi/a$ is the maximal wave-vector value (we first consider the results for \mathbf{k} directed along a cell edge). These trends qualitatively agree with the 2D case [23]. However, as the zero wave-vector diffusion coefficient in the 3D case is larger, SISF now decreases faster with time.

The preexponential $D_{s0}(t)$ factor in Eq. (9) is the limit of $D_s(k, t)$ when $k \rightarrow 0$:

$$D_{s0}(t) = \lim_{k \rightarrow 0} D_s(k, t). \quad (15)$$

Since the values for $k = 0$ are inaccessible in Monte Carlo simulations, the results for $k = \pm 1$ and ± 2 were approximated by parabolas and the values of $D_{s0}(t)$ were subsequently calculated. Thus all simulation data can be approximated by three time-dependent parameters, namely, $D_{s0}(t)$, $B_m(t)$, and $\kappa(t)$. All three functions are approaching their saturation values in the long-time limit. The zero wave-vector mean diffusion coefficient in the 3D case [Figs. 1(b), 2, and 3] is described by

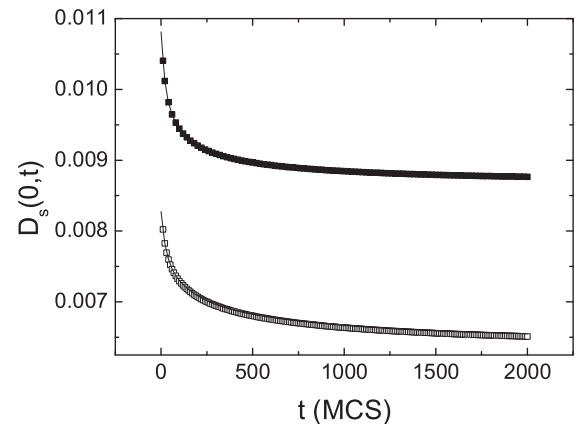


FIG. 2. Mean tracer diffusion coefficient at $k = 0$ versus time. $\theta = 0.5$, $T = 1.2T_c$ (full symbols), and $T = 1.05T_c$ (empty symbols). Solid lines for the two temperatures are drawn according to Eq. (16).

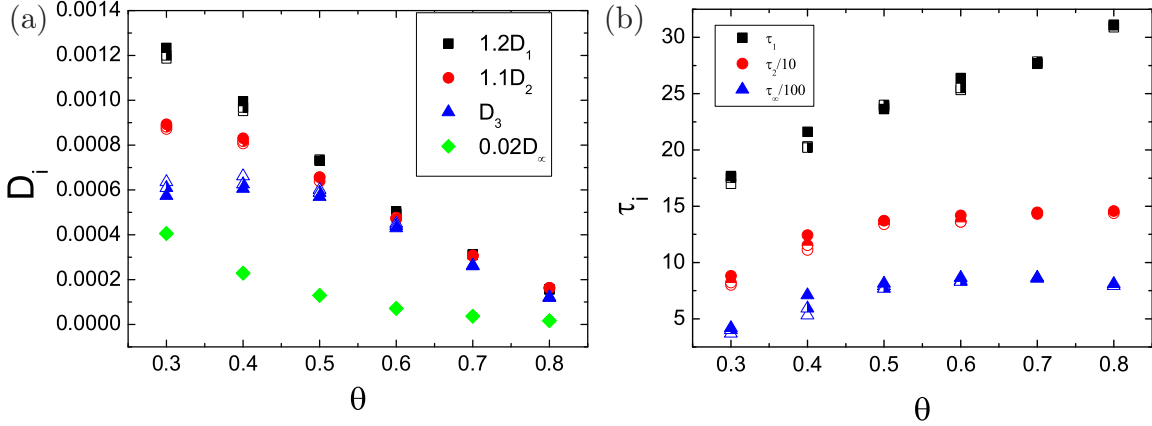


FIG. 3. (Color online) (a) Preexponential coefficients and (b) the relaxation times for the mean tracer diffusion coefficient as given by Eq. (16) at $k = 0$ versus lattice concentration at $T = 1.05T_c$ for the three characteristic directions: full symbols for the axes, semifilled for the face diagonals, and empty for the cubic diagonals.

three exponentially decaying functions

$$D_{s0}(t) = D_\infty + D_1 \exp(-t/\tau_1) + D_2 \exp(-t/\tau_2) + D_3 \exp(-t/\tau_3), \quad (16)$$

with approximately equal preexponential factors. When compared to the 2D case an additional short relaxation time in the range of 18–32 MCS appeared and the larger relaxation times are approximately 20% smaller and show stronger concentration dependence, mostly increasing with concentration. This means that the 3D lattice fluid relaxation is faster. Anisotropy of the preexponential factors is stronger at low concentrations and almost completely disappears at half coverage. In the limit of long times the anisotropy of the zero wave-vector mean diffusion coefficient does not appear at all.

For the 2D case it was possible to approximate $B_m(t)$ and $\kappa(t)$ by exponentially decaying functions; in the 3D case these quantities show a stretched exponential decay

$$\kappa(t) = \kappa_\infty + \kappa_1 \exp(-t^{\kappa_2}), \quad (17)$$

$$B_m(t) = B_\infty + B_1 \exp(-t^{B_2}). \quad (18)$$

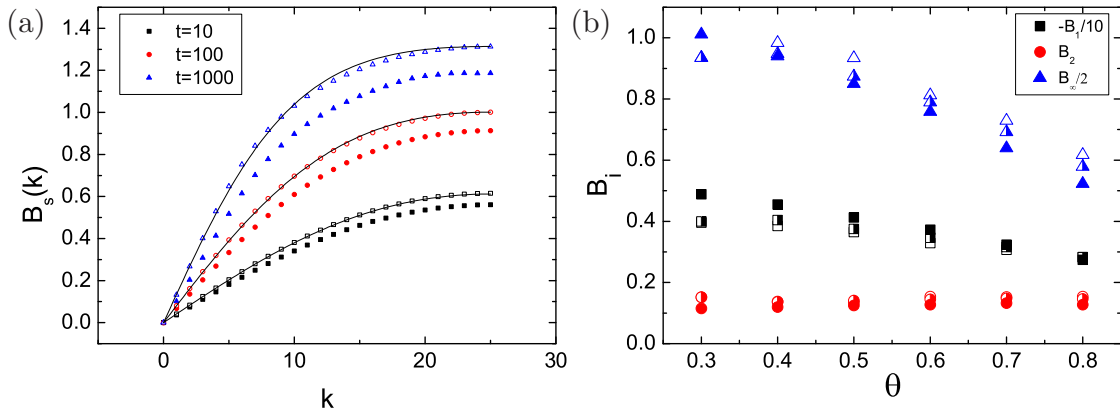


FIG. 4. (Color online) (a) Function B versus the wave vector directed along a cell edge for three different times. $\theta = 0.5$, $T = 1.2T_c$ (full symbols), and $T = 1.05T_c$ (empty symbols). Time t is given in MCS. Solid lines are drawn according to Eq. (7) and only for the data of $T = 1.05T_c$ and not for $T = 1.2T_c$ (for clarity in the figure). (b) The concentration dependences of the fitting parameters at $T = 1.05T_c$ for the three characteristic directions: full symbols for the axes, semifilled for the face diagonals, and empty for the cubic diagonals.

Figure 4(a) shows the k dependence of function B for three different times. Its behavior is well described by Eqs. (10) and (11). At small k , B shows linear dependence on k . The three fitting parameters (B_1, B_2 and B_∞) are shown in Fig. 4(b). B_1 is negative; however, at $t = 1$ MCS, B_m becomes positive and we do not consider $t < 1$ MCS. Again, we see weak concentration dependence of the parameters and their anisotropy is also weak, especially for the exponent B_2 that is approximately close to 0.15.

κ is an important scaling parameter that governs the wave-vector dependence of the diffusion coefficient and SISF. The preexponential factor of this parameter shows (Fig. 5) significant anisotropy and varies in the range of 450 to 900. Initially, large κ values relax to an order of magnitude smaller κ_∞ values. This means that the curvature of $B(k)$ curves increases with time as is evident from Fig. 4(a). Long-time limiting ξ_m values vary approximately in the range of 0.5 to 0.3 and the lowest values are for cube edges and thus anisotropy of the first Brillouin zone is significantly reduced as for a cubic lattice the ratios of the diagonals to the cube edge are $\sqrt{3}:\sqrt{2}:1$. At the same time, the exponent κ_2 does not show significant concentration dependence as well as anisotropy, and is approximately equal to 0.2.

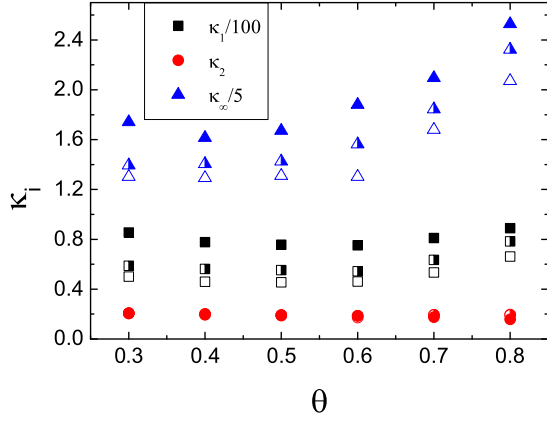


FIG. 5. (Color online) κ parameters for $T = 1.05T_c$ as a function of concentration for the three characteristic directions: full symbols for the axes, semifilled for the face diagonals, and empty for the cubic diagonals.

The temperature dependence of the characteristic parameters was then investigated as well. The preexponential factors of the fastest and the slowest contributions to the zero wave-vector mean tracer diffusion coefficient increase with temperature just as its long-time limit, while the middle contribution decreases [Fig. 6(a)]. At $T = 1.05T_c$ all contributions are equal to each other. The relaxation times weakly decrease with increasing temperature [Fig. 6(b)].

The B_m and κ parameters show weak and quite regular temperature dependence and weak anisotropy as well (Fig. 7). The exponents have low values, almost independent of temperature.

In Fig. 8 the hydrodynamic value of the mean tracer diffusion coefficient (at $k = 0$ and $t \rightarrow \infty$) is compared with the results of Monte Carlo simulations through the particle mean-square displacement (MSD), as given by the expression

$$\langle(\Delta \mathbf{r})^2\rangle = 6D_\infty t, \quad (19)$$

where time is given in MCS and the mean-square displacement in squared lattice spacing.

The agreement between all diffusion coefficients is considerably better than in the case of the 2D system because of larger

diffusion coefficients and faster relaxation in the 3D case. Thus in the time period of 2000 MCS the relaxation processes are diminished almost completely.

Faster diffusion and relaxation in 3D systems are concerned with a more developed group of diffusion trajectories that quantitatively is reflected through the entropy contribution [24–26]. We may speculate that this trajectory diversity in 3D systems leads to a wide spectrum of relaxation times that can be represented by stretched exponents as it is observed for relaxation of B_m and κ parameters.

In the Appendix it is shown that the mean-square displacement of a particle during finite time t is given by the expression

$$\langle[\mathbf{r}(t)]^2\rangle = 6D_s(0,t)t = 6 \int_0^t \hat{D}_s(0,t')dt'. \quad (20)$$

Above it was more practical to operate with the mean diffusion coefficient and then the true diffusion coefficient can be calculated from the integral equation (5) according to the relation

$$\hat{D}_s(\mathbf{k},t) = D_s(\mathbf{k},t) + t \partial D_s(\mathbf{k},t)/\partial t. \quad (21)$$

From the last expression it follows that if the mean diffusion coefficient is represented as a sum of several exponentially decaying functions [Eq. (16)] then the expression for the true diffusion coefficient is more complicated. However, the MSD calculated according to Eq. (20) through the mean diffusion coefficient Eq. (16) has a wrong asymptotic at $t \rightarrow \infty$. It is a straight line with a right tangent (D_∞) going through the coordinate origin, while the simulation results show the line intersecting the positive part of the MSD axis. On the other hand, it is more reasonable to suggest that just the true diffusion coefficient is represented by exponentially decaying functions. According to Eq. (21), its preexponential factors should be smaller than that of the mean diffusion coefficient and the asymptote will intersect the MSD axis at the point

$$\zeta = 6 \sum_{j=1}^3 \hat{D}_j \tau_j. \quad (22)$$

If we adopt $\hat{D}_j = D_j$, then $\zeta = 1.97$ and 3.26 for $T = 1.05T_c$, $\theta = 0.3$, and $\theta = 0.5$, correspondingly, that can be compared

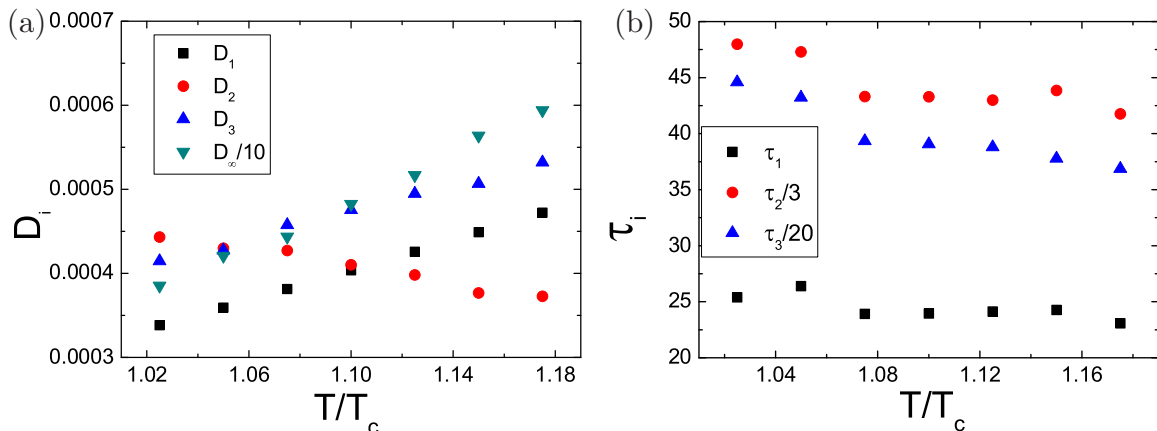


FIG. 6. (Color online) (a) Preexponential coefficients and (b) the relaxation times for the mean tracer diffusion coefficient as given by Eq. (16) at $k = 0$ versus temperature at $\theta = 0.6$ for axes directions.

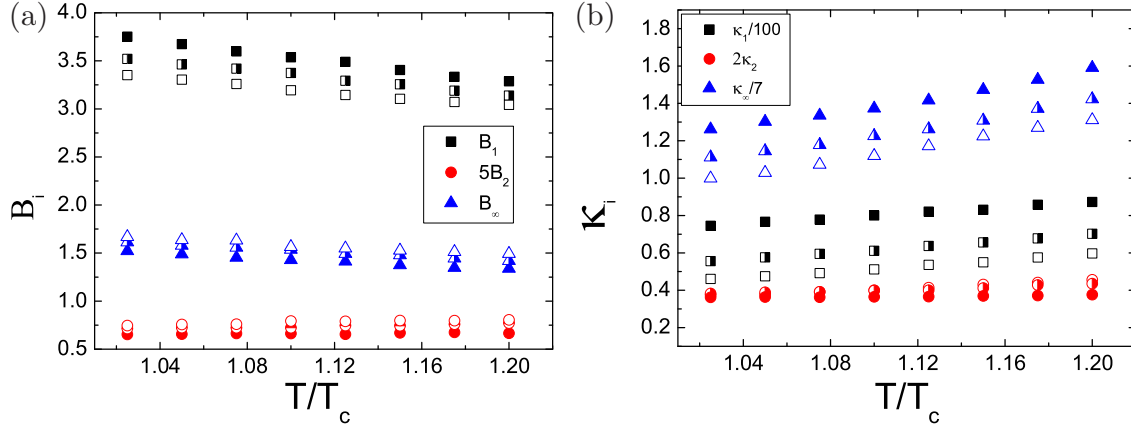


FIG. 7. (Color online) (a) κ parameters and (b) B_m parameters versus temperature at $\theta = 0.6$ for the three characteristic directions: full symbols for the axes, semifilled for the face diagonals, and empty for the cubic diagonals.

with the values 1.07 and 1.93 calculated from the MC simulation results. The difference between the results of Eq. (22) and the MC simulation results is explained by the fact that the preexponential factors of the mean diffusion coefficient were used. Just these values characterize the significance of the memory effects and we see that they correspond to rather small particle displacements of the order of the lattice spacing. Considerably larger deviations are expected for diffusion on fractal structures.

V. CONCLUSION

The simulation results for the self-intermediate scattering function (SISF) for a system of interacting particles on a 3D simple cubic lattice are given by a simple analytical expression with only one fitting parameter for representing its wave-vector dependence. All memory effects are included into the wave vector and time dependence of the diffusion coefficient.

The zero wave-vector mean tracer diffusion coefficient relaxation is governed by three relaxation times contrary to

the 2D case which has two relaxation times, with the largest one in the range of 750 to 1000 MCS. The two other parameters (the scaling parameter in the reciprocal space and B value at the boundary of the first Brillouin zone) cannot be described by a set of few exponentially decaying functions and show a stretched exponential decay with rather small exponents of the order $\alpha = 0.15$ to 0.2 . At $\alpha = 0.2$, 10^3 MCS are needed in order to complete 98% of the relaxation, while at $\alpha = 0.15$ 10^4 MCS are needed for this. For comparison, if relaxation is exponential 10^3 MCS and 10^4 MCS are necessary to complete relaxation by 98% for relaxation time 250 MCS and 2500 MCS, respectively. Thus the period of 2000 MCS used in the current investigation mainly covers the SISF relaxation to long-time behavior. The scaling parameter κ reduces the anisotropy of the first Brillouin zone and thus relaxation of the B parameter and the mean tracer diffusion coefficient is less anisotropic and the main anisotropy of SISF is provided by the geometric parameter η . The deviations of the particle MSD from straight lines $D_\infty t$ are of the order of the lattice spacing.

ACKNOWLEDGMENTS

This research has been cofinanced by the European Union (European Social Fund–ESF) and Greek national funds through the Operational Program “Education and Lifelong Learning” of the National Strategic Reference Framework (NSRF)—Research Funding Program: Heracleitus II (to L.S.) and Ministry of Education of Belarus (to V.V.).

APPENDIX

The equation for the MSD follows from Eqs. (2) and (3),

$$\frac{d\langle[\mathbf{r}(t)]^2\rangle}{dt} = - \int_V \mathbf{r} \cdot \mathbf{r} \frac{\partial}{\partial \mathbf{r}} \cdot \int_V \hat{D}_s(\mathbf{r} - \mathbf{r}', t) \frac{\partial G_s(\mathbf{r}', t)}{\partial \mathbf{r}'} d^3 \mathbf{r}' d^3 \mathbf{r}. \quad (\text{A1})$$

FIG. 8. (Color online) Comparison of the hydrodynamic value of the mean tracer diffusion coefficient (at $k = 0$ and $t \rightarrow \infty$) obtained after 2000 MCS with the results of Monte Carlo simulations through the particle mean-square displacement obtained after 10 000 MCS. $T = 1.05T_c$.

We consider here the tracer diffusion coefficient as a scalar quantity. Integrating by parts and assuming negligibly small values of the distribution function on the system boundary we

get

$$\begin{aligned}
 & \frac{d\langle[\mathbf{r}(t)]^2\rangle}{dt} \\
 &= - \int_V 2\mathbf{r} \cdot \int_V \hat{D}_s(\mathbf{r} - \mathbf{r}', t) \frac{\partial G_s(\mathbf{r}', t)}{\partial \mathbf{r}'} d^3\mathbf{r}' d^3\mathbf{r} \\
 &= - \int_V 2(\mathbf{r} - \mathbf{r}' + \mathbf{r}') \cdot \int_V \hat{D}_s(\mathbf{r} - \mathbf{r}', t) \frac{\partial G_s(\mathbf{r}', t)}{\partial \mathbf{r}'} d^3\mathbf{r}' d^3\mathbf{r} \\
 &= - \int_V 2(\mathbf{r} - \mathbf{r}') \hat{D}_s(\mathbf{r} - \mathbf{r}', t) d^3(\mathbf{r} - \mathbf{r}') \cdot \int_V \frac{\partial G_s(\mathbf{r}', t)}{\partial \mathbf{r}'} d^3\mathbf{r}' \\
 &\quad - 2 \int_V \hat{D}_s(\mathbf{r} - \mathbf{r}', t) d^3(\mathbf{r} - \mathbf{r}') \int_V \mathbf{r}' \cdot \frac{\partial G_s(\mathbf{r}', t)}{\partial \mathbf{r}'} d^3\mathbf{r}'. \quad (\text{A2})
 \end{aligned}$$

The first part of the last expression is equal to zero from the symmetry conditions or after integrating by parts. The second part after integration by parts and accounting of $\frac{d}{d\mathbf{r}'} \cdot \mathbf{r}' = n$, where n is the space dimensionality for the three-dimensional system, leads to the expression

$$\frac{d\langle[\mathbf{r}(t)]^2\rangle}{dt} = 6 \int_V \hat{D}_s(\mathbf{r} - \mathbf{r}', t) d^3(\mathbf{r} - \mathbf{r}') = 6\hat{D}_s(\mathbf{k} = 0, t) \quad (\text{A3})$$

and thus

$$\langle[\mathbf{r}(t)]^2\rangle = 6 \int_0^t \hat{D}_s(0, t') dt'. \quad (\text{A4})$$

-
- [1] R. Kutner, K. Binder, and K. W. Kehr, *Phys. Rev. B* **28**, 1846 (1983).
- [2] H. Spohn, *Large Scale Dynamics of Interacting Particles* (Springer, New York, 1991).
- [3] A. Danani, R. Ferrando, and E. Scalas, *J. Mod. Phys. B* **11**, 2217 (1997).
- [4] G. S. Bokun, Y. G. Groda, C. Uebing, and V. S. Vikhrenko, *Physica A* **296**, 83 (2001).
- [5] E. H. Feng and H. C. Andersen, *J. Chem. Phys.* **121**, 3598 (2004).
- [6] R. Gomer, *Rep. Prog. Phys.* **53**, 917 (1990).
- [7] M. C. Tringides and Z. Choj, *Collective Diffusion on Surfaces: Correlation Effects and Adatom Interaction* (Springer, New York, 2001).
- [8] A. R. Allnatt and A. B. Lidiard, *Atomic Transport in Solids* (Cambridge University Press, Cambridge, UK, 2004).
- [9] W. R. McKinnon and R. R. Haering, *Modern Aspects in Electrochemistry* (Plenum Press, New York, 1983).
- [10] M. D. Levi and D. Aurbach, *Electrochim. Acta* **45**, 167 (1999).
- [11] J. Bisquert, *Phys. Chem. Chem. Phys.* **10**, 49 (2008).
- [12] L. Onsager, *Phys. Rev.* **65**, 117 (1944).
- [13] J. P. Boon and S. Yip, *Molecular Hydrodynamics* (McGraw-Hill International, New York, 1980).
- [14] J. P. Hansen and I. R. McDonald, *Theory of Simple Liquids* (Academic Press, London, 1986).
- [15] A. Serra and R. Ferrando, *Surf. Sci.* **515**, 588 (2002).
- [16] P. A. Fedders and O. F. Sankey, *Phys. Rev. B* **18**, 5938 (1978).
- [17] R. A. Tahir-Kheli and R. J. Elliott, *Phys. Rev. B* **27**, 844 (1983).
- [18] R. A. Tahir-Kheli, *Phys. Rev. B* **27**, 6072 (1983).
- [19] H. van Beijeren and R. Kutner, *Phys. Rev. Lett.* **55**, 238 (1985).
- [20] E. Barsukov and J. R. Macdonald, *Impedance Spectroscopy. Theory, Experiment, and Applications* (John Wiley and Sons, Inc., Hoboken, NJ, 2005).
- [21] S. Kazlauskas, A. Kezionis, T. Salkus, and A. F. Orliukas, *Solid State Ion.* **231**, 37 (2013).
- [22] R. Kutner and K. W. Kehr, *Phys. Rev. B* **41**, 2784 (1990).
- [23] L. Skarpalezos, N. Tsakiris, P. Argyrakis, and V. S. Vikhrenko, *Phys. Rev. B* **84**, 075476 (2011).
- [24] T. M. Klarke and J. R. Durrant, *Chem. Rev.* **110**, 6736 (2010).
- [25] B. A. Gregg, *J. Phys. Chem. Lett.* **2**, 3013 (2011).
- [26] P. Giazitzidis, P. Argyrakis, J. Bisquert, and V. S. Vikhrenko, *Org. Electron.* **15**, 1043 (2014).